JACS
JOURNAL OF THE AMERICAN CHEMICAL SOCIETY

ARTICLE

pubs.acs.org/JACS

Charge Transfer Events in Semiconducting Single-Wall Carbon Nanotubes

Christian Oelsner,[†] M. Antonia Herrero,[‡] Christian Ehli,[†] Maurizio Prato,[*,§] and Dirk M. Guldi[*,†]

[†]Department of Chemistry and Pharmacy & Interdisciplinary Center for Molecular Materials, Friedrich-Alexander-Universität Erlangen-Nürnberg, Egerlandstrasse 3, 91058 Erlangen, Germany

[‡]Departamento de Química Orgánica — IRICA, Facultad de Química, Universidad de Castilla-La Mancha, 13071 Ciudad Real, Spain

[§]Dipartimento di Scienze Farmaceutiche & Center of Excellence for Nanostructured Materials, Università degli Studi di Trieste, Piazzale Europa 1, 34127 Trieste, Italy

Supporting Information

ABSTRACT: Electron-donating ferrocene units have been attached to SWNTs, with different degrees of functionalization. By means of a complementary series of novel spectroscopic techniques (i.e., steady-state and time-resolved), we have documented that mutual interactions between semiconducting SWNT and the covalently attached electron donor (i.e., ferrocene) lead, in the event of photoexcitation, to the formation of radical ion pairs. In the accordingly formed radical ion pairs, oxidation of ferrocene and reduction of SWNT were confirmed by spectroelectrochemistry. It is, however, shown that only a few semiconducting SWNTs [i.e., (9,4), (8,6), (8,7), and (9,7)] are susceptible to photoinduced electron transfer processes. These results are of relevant importance for the development of SWNT-based photovoltaics.

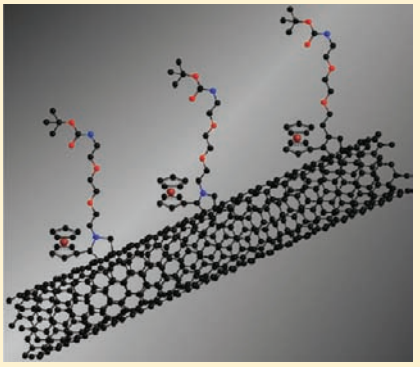

INTRODUCTION

Carbon nanotubes (CNTs) are emerging materials with high potential in several disciplines, in particular, electronics and photovoltaics.[1] Their unique structural features, such as high aspect ratio, have established them as novel materials in nanotechnology.[2] The structure and, in particular, the helicity determine the electronic and optical properties of a single-walled carbon nanotube (SWNT), the conductance, the lattice structure, and other properties.[3]

Because the helicity (chirality) dictates different electronic properties, we explored the role of "helicity" of SWNTs in charge transfer chemistry and evaluated the impact of functional groups/defects on the charge transport and, thereby, on the stability of the charge transfer product.[4]

The spectroscopic characterization of SWNTs and their metastable states is made difficult by the polydispersed nature of SWNT samples and the inevitable presence of SWNT in bundles of different sizes.[5] In addition, SWNTs are completely insoluble in organic and aqueous solvents, so that suitable methodologies for their dispersion are necessary.[6] To this aim, two general approaches, covalent functionalization[7] and noncovalent interactions,[8] are commonly used. The two approaches may eventually lead to similar results, but differ substantially in the change of hybridization from sp^2 to sp^3 in SWNT carbon atoms, which occurs only in the course of covalent functionalization. Heavy modification of this latter kind can therefore lead to an extensive loss of conjugation, with dramatic effects on electron acceptor and/or electron transport properties. This process can be monitored in the visible to the near-infrared region of the electronic absorption spectrum, where the characteristic van Hove singularities are present, due to the electronic transitions of the π-conjugated system. Alternatively, several hybrids have been prepared by the noncovalent adsorption of electron donors to SWNT,[9] utilizing supramolecular systems[10] such as $\pi-\pi$ stacking and/or electrostatic interactions,[11] while keeping the sp^2 character of the SWNT network intact.

In principle, the control of the degree of functionalization might be a suitable way for retaining the physicochemical properties of SWNTs, while allowing the association of a sufficient number of organic addends. This control is not always easy, as it depends on the nature of SWNTs, the type of reaction employed, and the reaction conditions. We have recently shown that the 1,3-dipolar cycloaddition of azomethine ylides is a milder reaction than the radical arylation, as it affects less the extended π-system of SWNTs.[7e] On the other hand, in earlier work, we had reported the preparation of the first SWNT-based hybrid material with electroactive moieties, ferrocene units extending from an ethyleneglycol chain attached to the nitrogen of the pyrrolidine ring.[12] The photophysical evaluation of that hybrid

Received: June 2, 2011
Published: October 31, 2011

Scheme 1. Structures of SWNT-Fc (3), SWNT-Fc (4), and SWNT-phenyl (5)

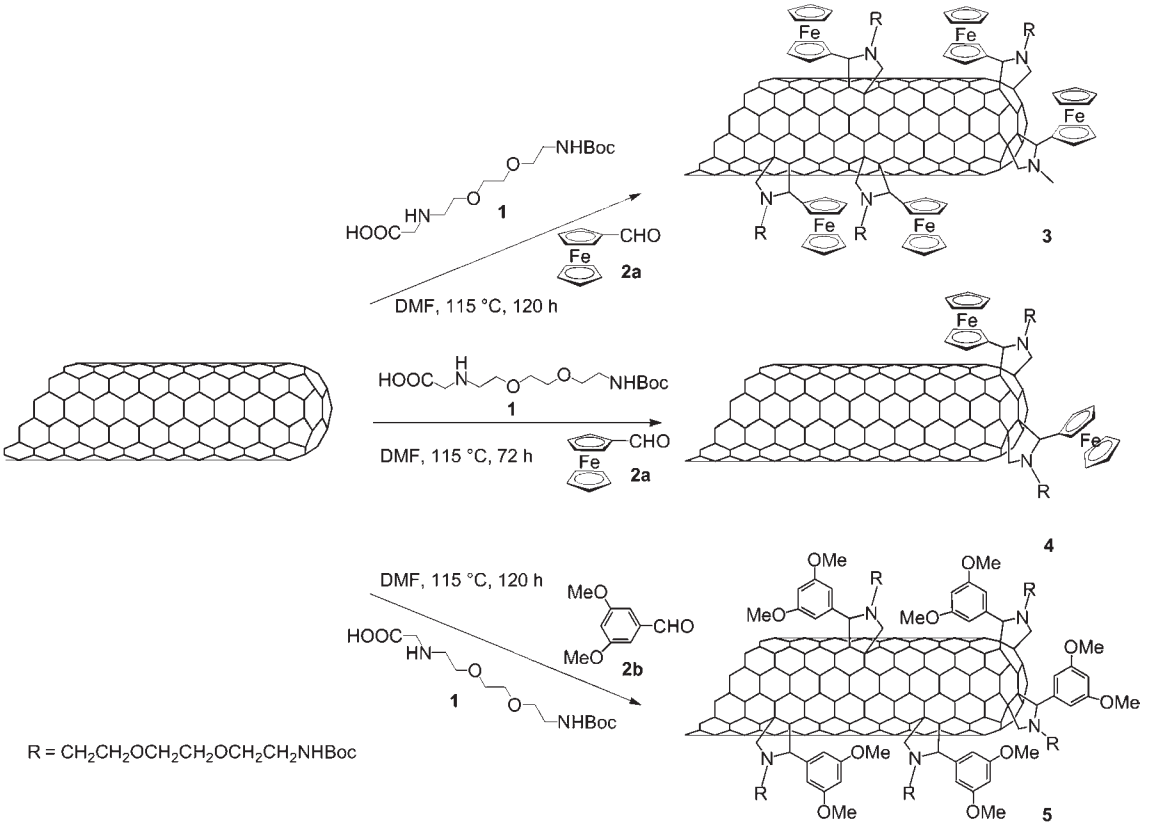

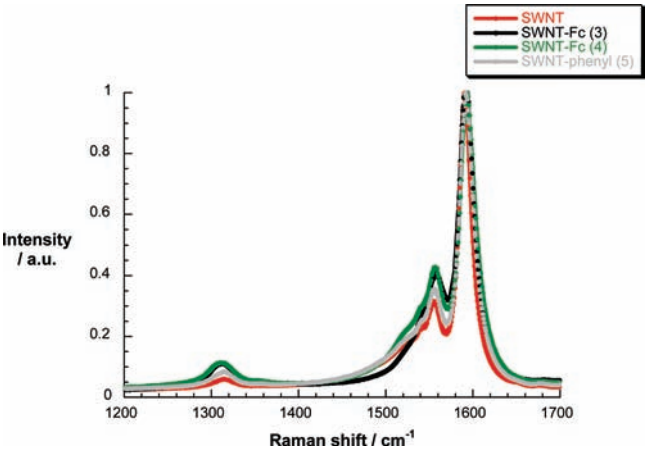

Figure 1. Raman spectra of SWNT (red spectrum), SWNT-Fc (**3**) (black spectrum), SWNT-Fc (**4**) (green spectrum), and SWNT-phenyl (**5**) (gray spectrum).

material revealed its great potential toward the construction of solar cells. However, in that case, due to the peculiar reactivity of the batch of SWNTs used, the covalent grafting of a plethora of ferrocene units onto the skeleton of SWNTs was achieved. Although the comprehensive characterization and the solution study of the material was possible, it was clear that the material had lost most of its electronic properties, as excited-state electron acceptor, and ferrocene, as ground-state electron donor.

In the present work, we employ the 1,3-dipolar cycloaddition of azomethine ylides to graft different quantities of ferrocene onto SWNT, using a rigid spacer to ensure a fixed and short distance between the SWNT surface. We demonstrate, for the first time, the electron transfer activity in individual SWNT, charge separation and charge recombination, as a function of SWNT type and as a function of SWNT functionalization. In practice, without the need to separate the SWNTs in groups of homogeneous chirality, we were able to discriminate the excited-state behavior of the entire batch. To this end, a benefit of the immobilized ferrocenes is their excellent reversible redox behavior, which enables the reversible modulation of their electron-donating ability by electrochemical oxidation. The results reported here are of primary importance when considering nanotechnological applications in solar energy conversion schemes.

RESULTS AND DISCUSSION

Ferrocene grafting to the SWNT sidewalls was performed using the 1,3-dipolar cycloaddition of azomethine ylides. The synthesis is sketched in Scheme 1. Three series of materials, SWNT-Fc (**3**), SWNT-Fc (**4**), and SWNT-phenyl (**5**), were prepared. SWNT-Fc (**3**) and SWNT-Fc (**4**) carry ferrocene units linked to the α-carbon of the pyrrolidine moiety with different degrees of functionalization. We have learned that, by fine-tuning the reaction conditions, we can modulate the extent of functionalization. In the present case, to limit the number of functional groups on SWNTs, we shortened the reaction times (see below). As a reference, in SWNT-phenyl (**5**), phenyl units were attached at the α-carbon of the pyrrolidine rings instead of the ferrocene

dx.doi.org/10.1021/ja205084x |*J. Am. Chem. Soc.* 2011, 133, 18696–18706

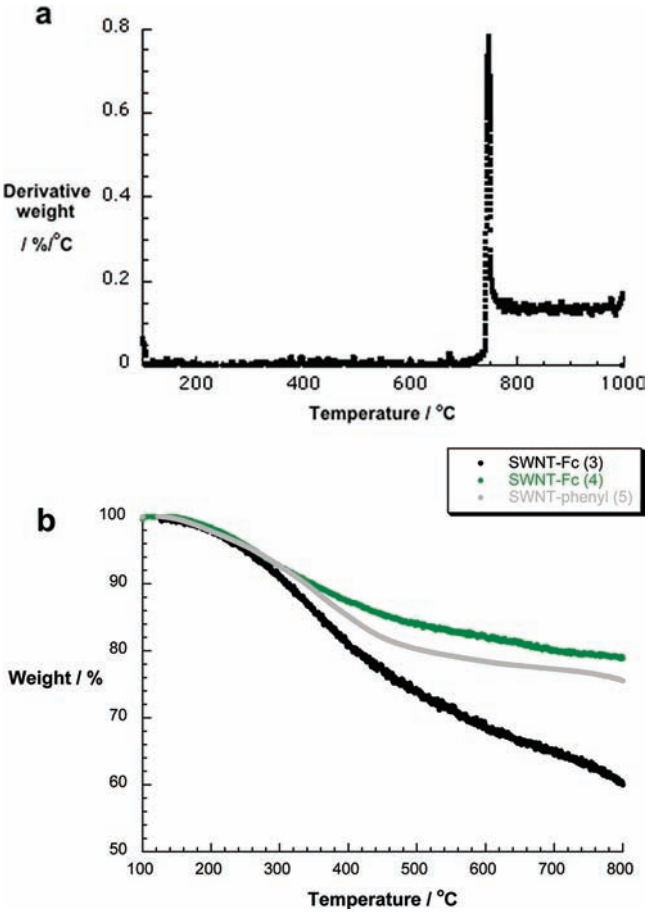

Figure 2. (a) First derivative of weight of pristine SWNT as a function of temperature, and (b) TGA curves of SWNT-Fc (**3**) (black spectrum), SWNT-Fc (**4**) (green spectrum), and SWNT-phenyl (**5**) (gray spectrum) recorded under inert conditions.

units. In brief, SWNT, amino acid **1** and aldehyde **2a** or **2b** were heated in DMF at 115 °C for a period of 5 days to yield SWNT-based materials **3** and **5**, respectively. On the contrary, compound **4** was prepared after only 3 days of heating using aldehyde **2a**. The functionalized materials, SWNT-Fc (**3**), SWNT-Fc (**4**), and SWNT-phenyl (**5**), were purified upon filtration on a Teflon filter. Subsequent washing of the black solid with cycles of sonication and filtration using DMF, methanol, and dichloromethane allowed removal of the excess reagents and byproducts.

The attenuated-total-reflectance IR (ATR-IR) spectra of SWNT-phenyl (**5**) and SWNT-Fc (**3** and **4**) provide evidence for the characteristic vibrations of the attached groups; see Figure S1. In particular, the $\nu(CH_2/CH_3)$ and $\delta(CH_2/CH_3)$ can be seen at 2970−2900 and 1395 cm^{-1}, respectively. In addition, the $\nu(C-N)$ occurs at 1250−1230 cm^{-1}, while the strong C−O−C valence vibrations are at 1053 cm^{-1}.

In Raman spectroscopy, typical spectra of SWNT-phenyl (**5**) and SWNT-Fc (**3** and **4**) are dominated by two bands, the D- and G-bands at 1311 and 1593 cm^{-1}, respectively. As documented in Figure 1, a significant enhancement of the D-band intensity (i.e., 1311 cm^{-1}) occurs upon functionalization. The increase of the D/G ratio confirms the transformation of sp^2- into sp^3-hybridized carbon atoms, as a result of the successful reaction. Importantly, the D/G ratio turned out to be higher in

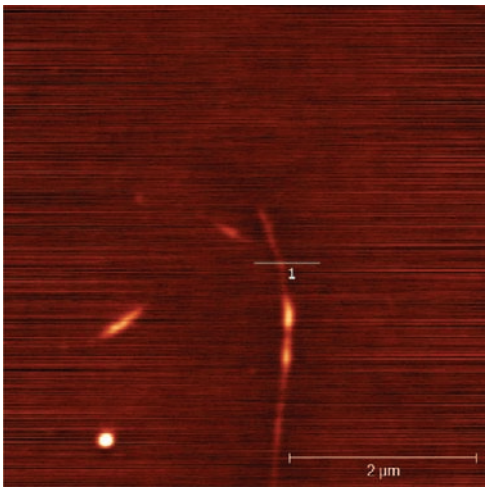

Figure 3. AFM image of a SWNT-Fc (**4**)/SDBS dispersion in D_2O.

SWNT-Fc (**3**) than in SWNT-Fc (**4**), a result that is well in line with the thermogravimetric analysis (TGA), vide infra.

SWNT-phenyl and SWNT-Fc were subjected to TGA, which allows determination of the relative amount of organic functionalities attached to the CNT surface. At this temperature, and under inert atmosphere, it is assumed that all of the organic fragments are removed, while the SWNT skeleton is still resistant; for illustration, see the first derivative spectrum of SWNT.[13] Typical thermographs, as they are presented in Figure 2, reveal weight losses of 29% (SWNT-Fc (**3**)), 19% (SWNT-Fc (**4**)), and 21% (SWNT-phenyl (**5**)). Accordingly, we conclude that one unit of the corresponding organic fragment is attached per every 129 carbon atoms in SWNT-phenyl (**5**), every 163 carbon atoms in SWNT-Fc (**4**), and every 94 carbon atoms in SWNT-Fc (**3**). These numbers are purely indicative, as the curves do not reach a steady plateau. However, a less rapid slope is clearly visible, at least for SWNT-Fc (**4**) and for SWNT-phenyl (**5**). To compare the different degrees of functionalization, the corresponding weight losses were determined at 550 °C. Notable is that, in this particular temperature regime, the organic materials covalently linked to SWNTs are fully removed, while SWNTs remain intact. Corroboration of the latter came from Figure 2a, which illustrates the first derivative as a function of temperature for pristine SWNTs.

Transmission electron microscopy (TEM) provides insight into the morphology of the newly synthesized materials. Linear micrometer-long structures with diameters of a few nanometers corresponding to the phenyl and ferrocene modified materials are discernible in typical TEM photographs; see Figure S2. At first glance, no significant differences are noticed between the functionalized SWNTs and the pristine SWNTs. Nevertheless, apart from some debundling and unroping, a clear improvement of the SWNT dispersion can be appreciated.

The new SWNT-phenyl and SWNT-Fc conjugates were analyzed using steady-state absorption. In contrast to our previously probed SWNT-Fc, which was exhaustively functionalized,[12a] the currently investigated SWNT-phenyl and SWNT-Fc still exhibit the signatures of the characteristic van Hove singularities throughout the entire near-infrared region (i.e., 1000−1600 nm) when dispersed in DMF. Despite the presence of functional groups, the electronic structure is largely preserved,

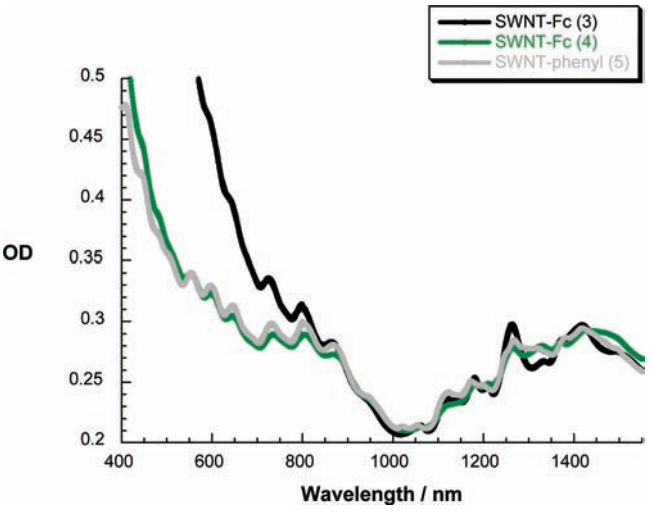

Figure 4. Absorption spectra of SWNT-Fc (**3**) (black spectrum), SWNT-Fc (**4**) (green spectrum), and SWNT-phenyl (**5**) (gray spectrum) in SDBS/D_2O.

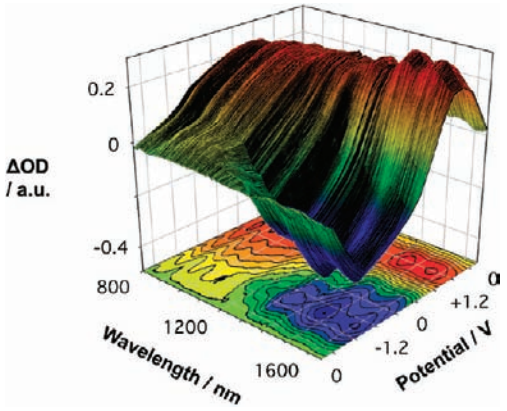

Figure 5. 3D-plot and 2D-plot of the differential results (red, increase in relative absorption/blue, decrease in relative absorption) from spectroelectrochemistry of SWNT-Fc (**4**) in SDBS/DMSO (0.1 M tetrabutylammonium hexafluorophosphate supporting electrolyte). All potentials were applied vs Ag wire.

a consequence that underlines a carefully controlled degree of SWNT functionalization.

To obtain deeper structural information, all SWNT samples were dispersed in D_2O with the help of sodium dodecylbenzylsulfonate (SDBS). This allows recording the absorption and fluorescence spectra with an improved resolution as compared to DMF. Ensuring the homogeneity of the functionalized SWNT suspensions is critical. To this end, atomic force microscopy is important, because it provides important insights into this aspect. Throughout the scanned areas, predominantly short (i.e., 1−5 μm) and very thin bundles (i.e., 2.3 nm) are discernible, Figures 3, S3, and S4, securing the fact that the functionalized SWNTs are well dispersed and individualized. In short, the functionalization proved to be beneficial in the exfoliation and individualization of SWNTs.

When analyzing the absorption spectra, especially in the red region (i.e., >900 nm), of SWNT and SWNT-phenyl (**5**), some interesting changes are unveiled; see Figure 4. Overall, some transitions are red-shifted from 1053, 1120, 1196, 1267, 1413,

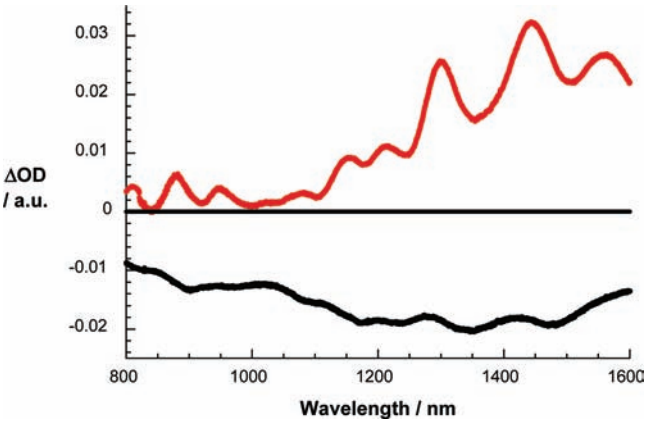

Figure 6. Differential absorption changes upon reduction (black spectrum) and oxidation (red spectrum) of SWNT-phenyl (**5**) in SDBS/DMSO (0.1 M tetrabutylammonium hexafluorophosphate supporting electrolyte).

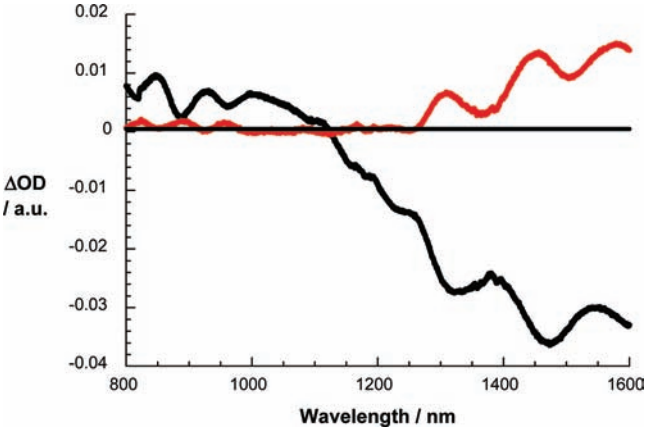

Figure 7. Differential absorption changes upon reduction (black spectrum) and oxidation (red spectrum) of SWNT-Fc (**4**) in SDBS/DMSO (0.1 M tetrabutylammonium hexafluorophosphate supporting electrolyte).

and 1494 nm in SWNT to 1053, 1122, 1197, 1268, 1414, and 1494 nm in SWNT-phenyl (**5**). This trend is quantitatively similar to what has been seen experimentally, upon chemically doping SWNT, and theoretically established, calculating the band gap in functionalized SWNT.[14] Because of the rather mild conditions of the 1,3-dipolar cycloaddition of azomethine ylides, the spectra are well resolved and still exhibit SWNT characteristics. Taking together all of these considerations, we postulate a homogeneous distribution of functionalized groups onto different types of SWNTs.

It is interesting to note that the attachment of the electron-donating ferrocene moieties leads to further red-shifts in the absorption characteristics to 1060, 1129, 1209, 1263, 1418, and 1550 nm in SWNT-Fc (**3**) and SWNT-Fc (**4**). Such an observation suggests appreciable electronic communication between the electron-donating ferrocenes and SWNTs. Here, the short donor−acceptor distance is thought to be responsible for the electronic coupling. It is interesting to note that the presence of more ferrocene units along the sidewalls of SWNT, SWNT-Fc (**3**) versus SWNT-Fc (**4**), leads to slightly better resolved

dx.doi.org/10.1021/ja205084x |*J. Am. Chem. Soc.* 2011, 133, 18696–18706

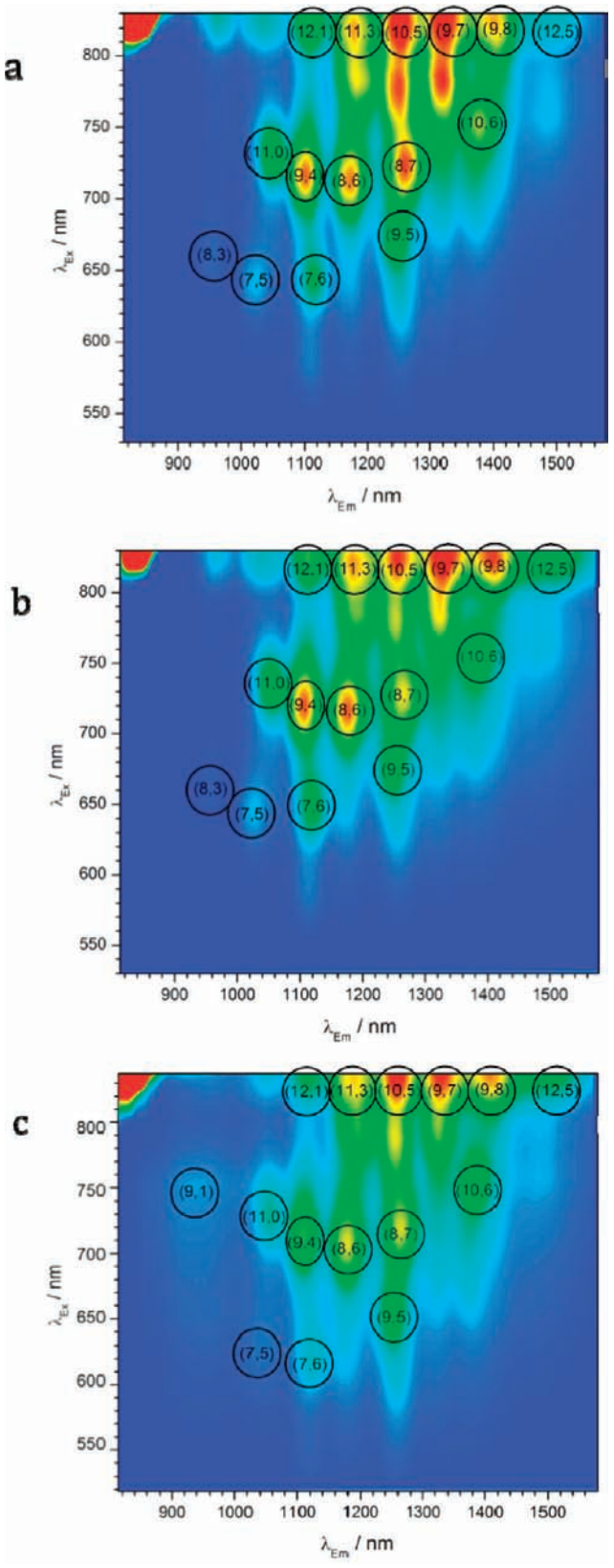

Figure 8. (a) Steady-state fluorescence spectra (3D), with increasing intensity from blue to green to yellow and to red, of SWNT in SDBS/D_2O (i.e., normalized by a factor of 2). (b) Steady-state fluorescence spectra (3D), with increasing intensity from blue to green to yellow and to red, of SWNT-phenyl (**5**) in SDBS/D_2O. (c) Steady-state fluorescence spectra (3D), with increasing intensity from blue to green to yellow and to red, of SWNT-Fc (**3**) in SDBS/D_2O.

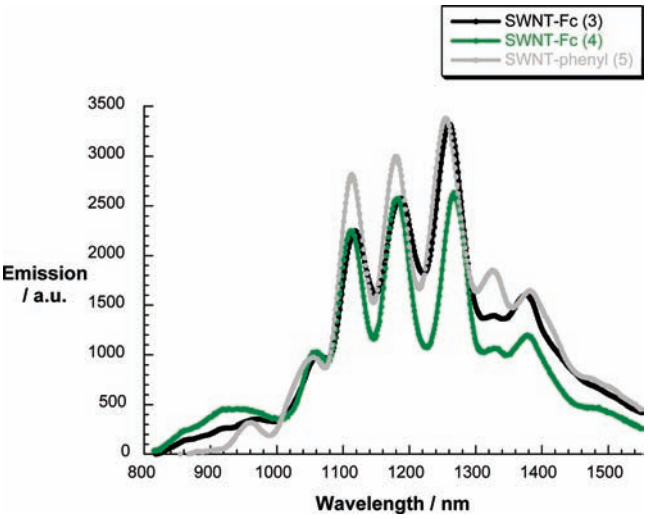

Figure 9. A comparison of fluorescence spectra of SWNT-Fc (**3**) (black spectrum), SWNT-Fc (**4**) (green spectrum), and SWNT- phenyl (**5**) (gray spectrum) in SDBS/D_2O with equal absorption at the excitation wavelength of 686 nm.

spectra, a fact that we attribute to an overall more homogeneous impact on the electronic coupling with SWNTs.

Before turning to the emission measurements, we focused on establishing in situ spectroscopic signatures associated with the charge transfer chemistry of SWNT suspensions and on exploring the overall reversibility of the underlying processes. With the application of cathodic potentials, going from 0 to −1.2 V and back to 0 V (vs Ag wire), a reversibly occurring decrease and increase in absorption, respectively, is observed in the 1000−1600 nm range, where the van Hove singularities of the semiconducting SWNT-Fc (**3**), SWNT-Fc (**4**), and SWNT-phenyl (**5**) are located, Figure 5. Figures 6 and 7 allow a closer look revealing subtle changes during the reductive conditions for SWNT-phenyl (**5**) with minima at 835, 900, 970, 1105 (9,4), 1175 (8,6), 1240 (8,7), 1350 (9,7), 1475, and 1600 nm, as well as for SWNT-Fc (**4**) with minima at 820, 885, 955, 1055, 1110 (9,4), 1180 (8,6), 1260 (8,7), 1320, 1360 (9,7), 1475, and 1600 nm. Second, transitions located in the red part of the visible spectrum (i.e., 1418 and 1558 nm) start to change at lower applied potentials than those at lower wavelength (i.e., 1066 and 1120 nm). This is an important observation, because it indicates that the smaller band gap SWNTs (i.e., absorbing in the red) are reduced more easily, that is, at less negative potentials when compared to those SWNTs that possess larger band gaps (i.e., absorbing at lower wavelength in the visible spectrum). Third, during the back scans, the larger band gap SWNTs (i.e., absorbing at lower wavelength in the visible spectrum) are more susceptible toward reoxidation than SWNT with smaller band gaps (i.e., absorbing in the red). In SWNT-Fc (**3**), the same trends were realized.[15] All of these changes are quantitatively reversed when resetting the potential to 0 V (vs Ag wire). Finally, under oxidative conditions, SWNT-phenyl (**5**) gives rise to maxima at 810, 880, 945, 1080, 1155, 1215, 1298, 1445, and 1560 nm, while maxima at 825, 890, 955, 1085, 1165, 1220, 1310, 1455, and 1580 nm evolve for SWNT-Fc (**4**). Reference experiments with SWNT led essentially to a qualitatively similar picture.[14a,c]

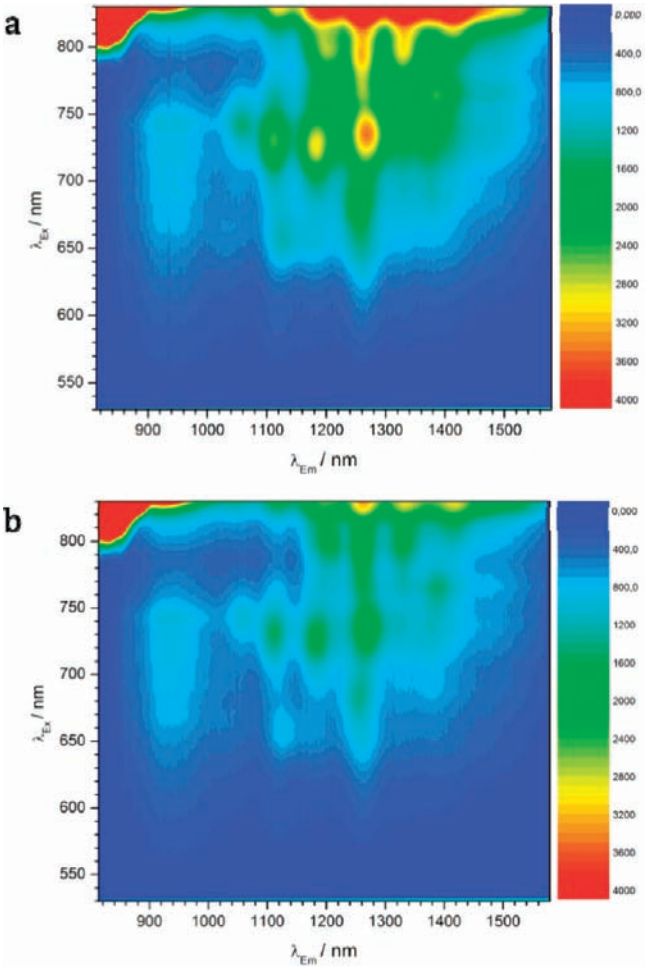

Figure 10. (a) Steady-state fluorescence spectra (3D), with increasing intensity from blue to green to yellow and to red, of SWNT-Fc (**4**) in SDBS/D_2O at +0.4 V (vs Ag wire). (b) Steady-state fluorescence spectra (3D), with increasing intensity from blue to green to yellow and to red, of SWNT-Fc (**4**) in SDBS/D_2O at −0.4 V (vs Ag wire).

As a complement to the absorption spectra, 3D fluorescence spectra were taken. Figure 8a reports the 3D fluorescence spectrum of SWNTs. These spectra are very informative, because all of the peaks have been assigned to specific helicity tubes, so that the composition of the mixture under study can be discerned.[16] In our case, SWNT exhibits the strongest fluorescence maxima, ascribed to (9,4), (7,6), (8,6), (11,3), (9,5), (10,5), (8,7), and (9,7) SWNT. For SWNT-phenyl (**5**), a 3D fluorescence landscape, (8,3), (7,5), (7,6), (9,5), (10,2), (9,4), (8,6), (8,7), (12,1), (10,5), (9,7), (9,8), (10,6), and (12,5), evolves with appreciable bathochromic shifts when compared to SWNT; see Figure 8b. For example, the 1197 and 1414 nm maxima shift to 1209 and 1418 nm, respectively. All of the associated shifts parallel those seen in the absorption spectrum.

Next, the 1100−1500 nm range was employed as a sensitive probe to detect excited-state interactions between SWNT and ferrocene in SWNT-Fc (**3**) and SWNT-Fc (**4**). When comparing the fluorescence intensity of the landscapes at, for example, the maxima at 1209 and 1428 nm, the following trend is deduced: SWNT > SWNT-phenyl (**5**) > SWNT-Fc (**4**) ≈ SWNT-Fc (**3**). In addition to the 3D fluorescence landscapes, emission spectra of SWNT-phenyl (**5**), SWNT-Fc (**3**), and SWNT-Fc (**4**) were

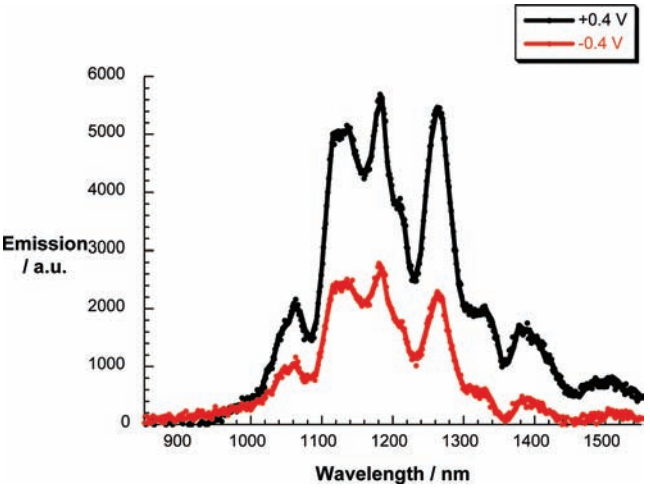

Figure 11. A comparison of fluorescence spectra taken at a potential of +0.4 V (black spectrum) and −0.4 V (red spectrum) of SWNT-Fc (**4**) in SDBS/D_2O with equal absorption at the excitation wavelength of 532 nm (laser excitation).

recorded with an excitation wavelength of 686 nm, which are shown in Figure 9. Interestingly, (9,4), (8,6), (8,7), and (9,7) give rise to significant fluorescence quenching. Up to 60% and 50% quenching relative to SWNT and SWNT-phenyl (**5**), respectively, was noted in SWNT-Fc (**3**) and SWNT-Fc (**4**). On the contrary, the fluorescence of (8,3), (7,5), (10,2), (10,6), and (12,5) does not seem to be affected by the presence of the ferrocene units. Interestingly, for those SWNTs that are not quenched, the overall fluorescence intensity seems higher in SWNT-Fc (**3**) than in SWNT-Fc (**4**). In fact, this trend resembles the ground-state features, where a larger number of ferrocenes and, in turn, a more homogeneous electronic coupling leads to better resolved features.

Further insight into the charge transfer evolving between photoexcited SWNT as the fluorescent probe and ferrocene came from faradaic modulation of the SWNT centered fluorescence, the repeated (i.e., 20 times) electrochemical reduction and oxidation of SWNT and SWNT-Fc in suspension. In previous work by Tanaka et al., redox potentials of individual (*n*,*m*) SWNTs were experimentally determined by electrofluorescence measurement of modified SWNT films.[17a] Also, chemical oxidation and reduction of SWNTs were probed by fluorescence measurements.[17b] In our own work, the potential-dependent fluorescence measurements were performed by redox switching in the range between −0.8 and +0.4 V (vs Ag wire). In SWNT-phenyl (**5**), linear scan voltfluorograms, Figure S5, reveal under both reductive and oxidative conditions a net decrease of fluorescent emission (i.e., 532 nm laser excitation) due to resonance loss. Importantly, during the measurements, no modulation of the SWNT concentration took place. Decisive is that in SWNT-Fc (**3**) and SWNT-Fc (**4**) the quenched fluorescence is reactivated upon electrochemical oxidation of ferrocene; please compare Figure 10a and b. Now, the fluorescence signal is proportional to the number of oxidized ferrocenium in SWNT-Fc. Rereducing the oxidized ferrocenium reinitiates the charge transfer and, in turn, eliminates once again the fluorescence quenching. At potentials less negative than the ferrocenium/ferrocene reduction, the loss of resonance, as the fluorescent SWNTs are getting charged, results in a further drop of the

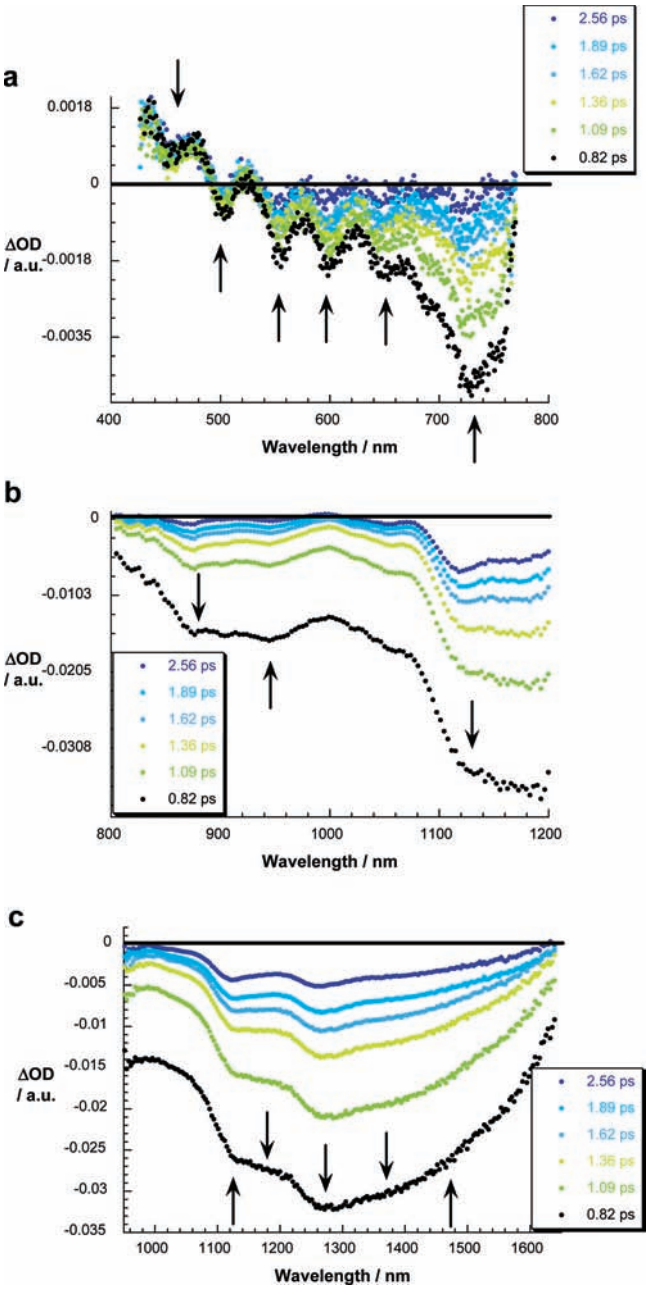

Figure 12. (a) Differential absorption spectra (visible) obtained upon femtosecond flash photolysis (387 nm) of SWNT-phenyl (**5**) in SDBS/D_2O with several time delays at room temperature; see figure legend for time delays; black arrows refer to the SWNT excited-state features. (b) Differential absorption spectra (near-infrared) obtained upon femtosecond flash photolysis (387 nm) of SWNT-phenyl (**5**) in SDBS/D_2O with several time delays at room temperature; see figure legend for time delays; black arrows refer to the SWNT excited-state features. (c) Differential absorption spectra (extended near-infrared) obtained upon femtosecond flash photolysis (387 nm) of SWNT-phenyl (**5**) in SDBS/D_2O with several time delays at room temperature; see figure legend for time delays; black arrows refer to the SWNT excited-state features.

fluorescence. Complementary inspection of the fluorescent SWNT generalized this trend, that is, the independence of the excitation wavelength, Figure 11.

In the final step of the characterization, SWNT, SWNT-phenyl, and SWNT-Fc were probed by means of transient

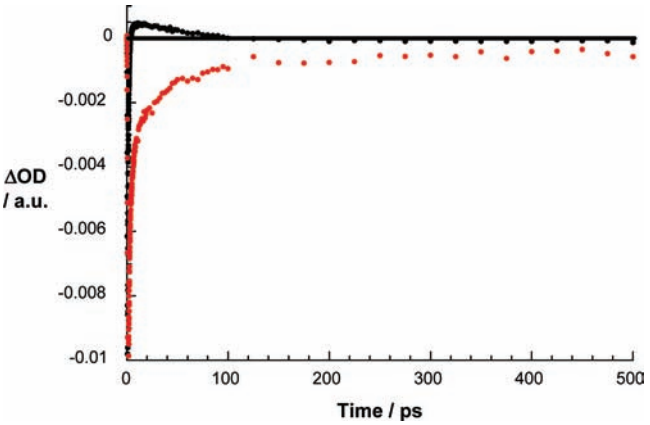

Figure 13. Time−absorption profiles of the spectra shown in Figure 12 at 1000 (black line) and 1125 nm (red line) monitoring the excited-state decay.

absorption spectroscopy. In particular, SDBS/D_2O suspensions of SWNT and SWNT-phenyl (**5**) were photoexcited at either 387 or 775 nm, and the spectral changes were recorded with time delays that typically ranged from 200 fs to about 3000 ps. Suspensions of either SWNT or SWNT-phenyl (**5**), which were used as internal reference points, gave rise to a transient bleach, with minima that are seen for SWNT-phenyl (**5**) at 456, 502, 554, 596, 644, 724, 880, 944, 1125, 1170, 1264, 1375, and 1480 nm, that is best described as an exact mirror image of the van Hove singularities in the visible and near-infrared, Figure 12. Importantly, the recovery of the ground state is not associated with any spectral changes (i.e., shifts, etc.) of the metallic and semiconducting SWNTs, whose transitions fall into the visible and near-infrared regions, respectively. Instead, all features decay similarly to recover the ground state with two major lifetime components (i.e., 2 and 65 ps), Figure 13.

Fundamentally different is the spectral behavior for SWNT-Fc (**4**), Figure 14, excited either at 387 or at 775 nm. Initially after the photoexcitation, a picture evolves that bears some resemblance with that noted for SWNT or SWNT-phenyl (**5**), a mirror image of the ground state. Considering the ground-state absorption, SWNT-Fc (**4**) reveals minima at 555, 600, 880, 940, 1055, 1125, 1185, 1275, 1338, and 1490 nm. These features decay in SWNT-Fc (**4**) within approximately 2 ps (7.7×10^{11} s^{-1}), which we tentatively assign to electron injection processes into semiconducting SWNT and is known from the literature.[18] We noted that, along with these accelerated decays, the transitions undergo uniform hypsochromic shifts. After the conclusion of the electron injection, the following features are discernible for SWNT-Fc (**4**): 550, 595, 710, 865, 955, 1055, 1120, 1180, 1260, and 1360 nm. The minima at 1120, 1180, 1260, and 1360 nm are of particular importance, because they relate to (9,4), (8,6), (8,7), and (9,7). In other words, the same SWNTs reveal appreciable changes in fluorescence intensity, for which we have determined charge transfer state energies ranging from −0.64 (9,7) to −0.73 eV (9,4).[17a] A similar picture evolves for SWNT-Fc (**3**), Figure S6, with 935, 1050, 1073, 1125, 1172, 1271, 1338, and 1490 nm minima that transform into a set of features at 935, 1050, 1134, 1175, 1263, and 1326 nm. Notably, such hypsochromically shifted transient features are (i) well in line with the spectroelectrochemistry and (ii) have been monitored in

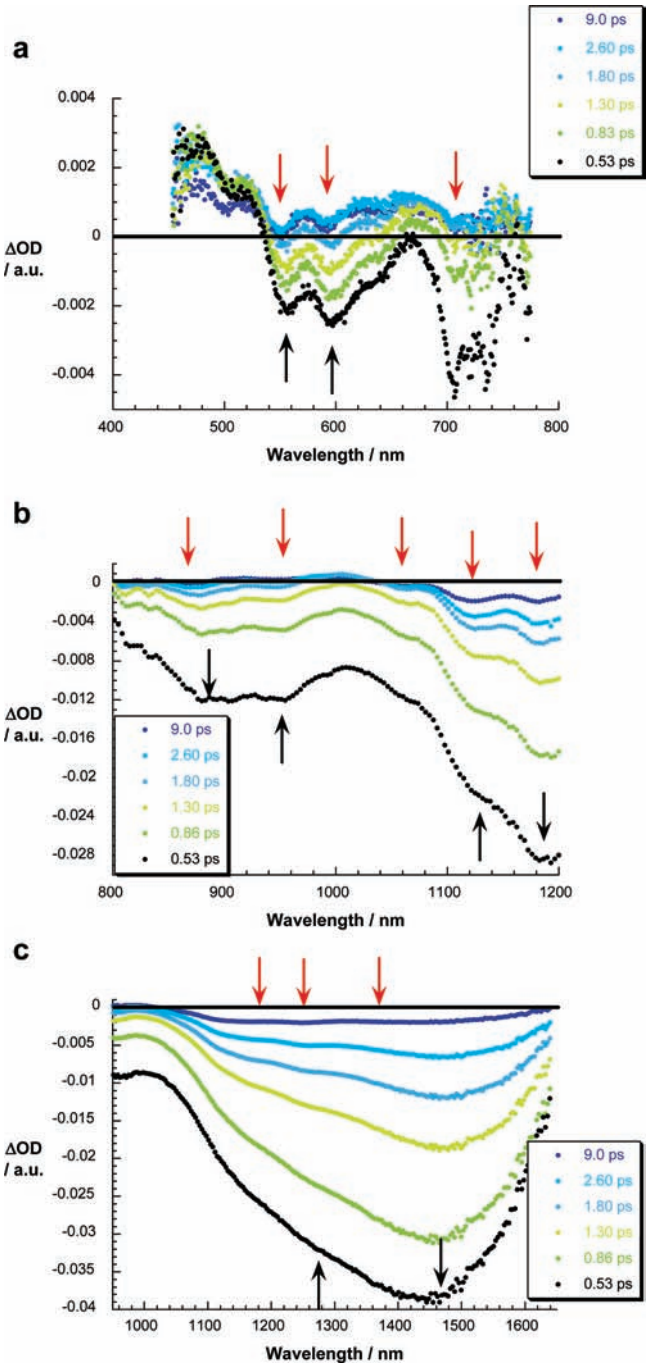

Figure 14. (a) Differential absorption spectra (visible) obtained upon femtosecond flash photolysis (387 nm) of SWNT-Fc (**4**) in SDBS/D_2O with several time delays between 0 and 10 ps at room temperature; see figure legend for time delays; black arrows refer to the SWNT excited-state features; red arrows refer to the SWNT charge transfer state. (b) Differential absorption spectra (near-infrared) obtained upon femtosecond flash photolysis (387 nm) of SWNT-Fc (**4**) in SDBS/D_2O with several time delays between 0 and 10 ps at room temperature; see figure legend for time delays; black arrows refer to the SWNT excited-state features; red arrows refer to the SWNT charge transfer state. (c) Differential absorption spectra (extended near-infrared) obtained upon femtosecond flash photolysis (387 nm) of SWNT-Fc (**4**) in SDBS/D_2O with several time delays between 0 and 10 ps at room temperature; see figure legend for time delays; black arrows refer to the SWNT excited-state features; red arrows refer to the SWNT charge transfer state.

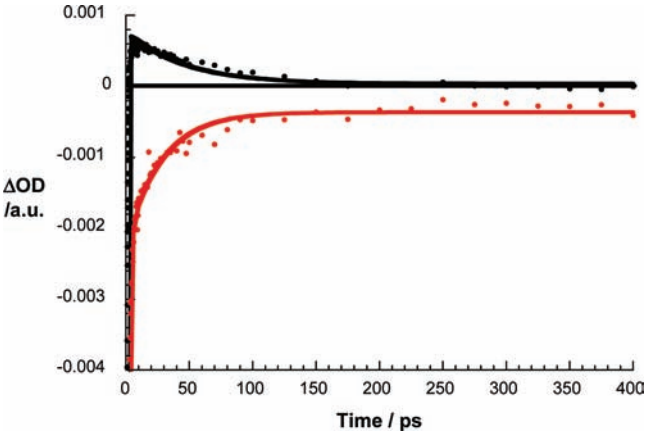

Figure 15. Time−absorption profiles of the spectra shown in Figure 14 at 985 (black line) and 1120 nm (red line) monitoring the formation of the radical ion pair state.

recent examples of SWNT electron donor−acceptor hybrids/conjugates that bear, for instance, excited-state electron donor moieties such as extended tetrathiafulvalene (exTTF) or zinc phthalocyanines (ZnPc).[19,20] Implicit are new conduction band electrons shifting the transitions to lower energies.[21] The charge transfer transients are metastable and recombine on a time scale of up to 200 ps, suggesting a rather efficient recombination of charge carriers. Quite interestingly, SWNT-Fc (**4**) gives rise to an appreciable stabilization of the charge transfer product when compared to SWNT-Fc (**3**) with lifetimes of 89 ps (1.1×10^{10} s^{-1}) and 21 ps (4.8×10^{10} s^{-1}), respectively, Figure 15. In terms of confirming the presence of the oxidized ferrocenium, we should direct our attention to the visible part of the spectrum; an illustrative example is shown in Figure 14. The broad and also weak absorption that is noted between 600 and 800 nm (i.e., with a maximum around 650 nm) is reminiscent to that reported for the one-electron oxidized ferrocenium.[22]

In summary, we have documented that the selective photoexcitation of SWNT in SWNT-Fc (**3**) and SWNT-Fc (**4**) is followed by a rapid charge transfer, the formation of reduced SWNT and oxidized ferrocene. The close spatial proximity between SWNT and the ferrocenes is the key to power a rapid charge transfer (i.e., 2 ps) and likewise to impact the charge recombination (i.e., 100 ps). Controlling the different redox states of the electron donor, ferrocene versus ferrocenium, with different potentials enabled the reversible redox switching of SWNT-Fc.

An obvious correlation of the charge transfer activity prompts one to inspect the helicities of SWNT-Fc. In this respect, it is interesting to note that the charge transfer active SWNT-Fc, (9,4), (8,6), (8,7), and (9,7), has rather large chirality angles that range from 25.3° to 27.8°, with the exception of (9,4) with 17.5°. In stark contrast, for those SWNT-Fc that lack charge transfer activity, that is, (8,3), (7,5), (10,2), (10,6), and (12,5), we have determined small chirality angles between 15.3° and 24.5°. Here, the exception seems to be (10,2) with 9.0°. The dependence on the chirality angles prompts us to the following considerations. Common to SWNT with larger chirality angles is their increasing arm-chair character. Please note that pure arm-chair SWNT with a chirality angle of 30° would be metallic and, thus, not identifiable by our fluorescence and transient absorption assays. Of particular relevance is the misalignment angle of the

π-orbitals in SWNT, which ultimately serve as the electron acceptor. In this regard, recent studies have correlated the misalignment angles (ϕ) for the inequivalent bonds in zigzag and arm-chair SWNT as it impacts the π-electron density in, for example, π-electron interactions/stacking. In general, the π-orbital misalignment angle tends to be smaller in arm-chair SWNT than in zigzag SWNT at a given diameter. In addition, in arm-chair SWNT, the π-electron density converges in the different π-electron interactions (i.e., stack form and stack form) with, for example, benzene as the SWNT diameter increases. On the contrary, the differences in the corresponding zigzag SWNT remain invariant as the diameter changes.

Less straightforward is the relationship between SWNT-Fc diameters and/or the corresponding band-gaps. Only the intermediately sized SWNT-Fc (i.e., 0.92−1.1 nm) is susceptible to accept electrons from ferrocene, while the smaller (i.e., 0.78−0.87 nm) and larger sized SWNT-Fc (i.e., 1.11−1.2 nm) are obviously inert toward charge transfer. A different line of arguments rationalizes the overall dependence on the diameter. Because of the fact that the electron transfer scenario evolves from photoexcited SWNT, the size quantization of SWNT is decisive as it exerts a significant impact on the electron transfer dynamics. In particular, in small diameter SWNT a per se larger energy gap favors a strongly exothermic electron transfer. The driving forces diminish as the diameter increases/band gap decreases. Very small diameter SWNTs play, however, no significant role on the basis of the aforementioned argument, leaving the intermediate diameter as the most electron transfer active SWNT.

Finally, the stability of the charge transfer product is linked to the degree of SWNT functionalization. In this regard, it is interesting to note that a higher degree of functionalization (i.e., one functional group every 94 carbon atoms versus every 163 carbon atoms), and, as a consequence, a larger number of defects onto SWNT, causes a significant destabilization of the charge transfer product (i.e., 21 versus 89 ps). It is likely that the injected conduction band electrons suffer from a reflection at these defect sites. Such a scenario exerts limitations to the charge delocalization and stands in stark contrast to the proposed ballistic conductance, which would necessitate structural perfection of SWNT.

CONCLUSIONS

In summary, by complementary spectroscopic and microscopic techniques, we could show mutual interactions between semiconducting SWNT and the covalent attached electron donor unit ferrocene by charge transfer processes and the formation of radical ion pairs, generated by photochemical means. Important is the establishment of a versatile methodology to achieve signatures of reduced/oxidized SWNT as they evolve in charge transfer reactions in novel chemical as well as light driven systems by spectroscopic and also the use of new in situ spectroelectrochemistry techniques, absorption and fluorescence spectroscopy. Moreover, the lifetimes of the radical ion pairs emerge as important benchmarks in the context of employing them for photoelectrochemical/photovoltaic solar energy conversion.

MATERIALS AND METHODS

General Methods. Steady state UV/vis/NIR absorption spectroscopy was performed by a Cary 5000 spectrometer (VARIAN) with a spectral resolution of 0.3 nm. Transient absorption spectroscopy was performed with 775 and 387 nm laser pulses of an amplified Ti/sapphire laser system (model CPA 2101, Clark-MXR Inc. − output: 775 nm, 1 kHz and 150 fs pulse width) in the TAPPS, transient absorption pump/probe system, Helios from Ultrafast Systems with 200 nJ laser energy. Steady-state fluorescence spectra were taken from samples by a FluoroLog3 spectrometer (HORIBA) with a IGA Symphony (512 × 1 × 1 μm) detector in the NIR detection range. The Raman spectra were run with a FT-Raman spectrometer RFS100 from Bruker with an excitation wavelength of 1064 nm and a liquid nitrogen cooled Germanium detector. Spectroelectrochemistry experiments were performed with a home-built cell and a three-electrode setup: a light-transparent platinum gauze as working electrode, a platinum wire as counter electrode, and a silver wire as quasi reference electrode. Potentials were applied and monitored with an EG&G Princeton Applied Research potentiostat (model 263 A). The path length of the cell was determined to 2.3 mm. The results are finally shown as differential spectra, that is, the difference between a spectrum with and without an applied potential. The spectra were recorded with a UV/vis/NIR spectrometer Cary 5000 (VARIAN), and a FluoroLog3 spectrometer (HORIBA) with a IGA Symphony (512 × 1 × 1 μm) detector in the NIR detection range. TEM analysis was performed by placing several drops of a solution of the SWNT dispersion on a copper grid (3.00 mm, 200 meshes). After vacuum drying overnight (10^{-2} bar), the sample was observed with a TEM Philips EM 208 microscope (accelerating voltage of 100 kV). AFM images were taken on a scanning probe microscope Solver Pro (NT-MDT Co). The carbon nanotube material was coated on a oxidized silicon wafer by spin coating and carefully washed two times with water for removing excessive SDBS.

Synthesis: SWNT-Fc (3). In a typical experiment, 30 mg of pristine SWNTs was suspended in DMF (30 mL) and sonicated for 30 min, and then the amino acid **1** (180 mg) and the ferrocenecarboxaldehyde **2a** (180 mg) were added in small quantities (45 mg every 24 h), and the reaction mixture was heated at 115 °C for 5 days. After being cooled to room temperature, the solution was filtered on a Millipore membrane (PTFE, 0.22 μm), and the black solid was washed several times with fresh DMF, MeOH, and CH_2Cl_2 (sonicated, centrifuged, and filtered) until the supernatant solution remained colorless. The solid on the filter was washed with diethyl ether, affording functionalized SWNTs **3** (27 mg). One functional group, each 94 atoms of carbon (29%), is calculated after analysis of TGA thermographs.

SWNT-Fc (4). In a typical experiment, 30 mg of pristine SWNTs was suspended in DMF (30 mL) and sonicated for 30 min, then the amino acid **1** (90 mg) and the ferrocenecarboxaldehyde **2a** (90 mg) were added portionwise (45 mg every 24 h), and the reaction mixture was heated at 115 °C for 3 days. After being cooled to room temperature, the solution was filtered on a Millipore membrane (PTFE, 0.22 μm), and the black solid was washed several times with fresh DMF, MeOH, and CH_2Cl_2 (sonicated, centrifuged, and filtered) until the supernatant solution remained colorless. The solid on the filter was washed with diethyl ether, affording functionalized SWNTs **4** (29 mg). One functional group, each 163 atoms of carbon (19%), is calculated after analysis of TGA thermographs.

SWNT-phenyl (5). In a typical experiment, 30 mg of pristine SWNTs was suspended in DMF (30 mL) and sonicated for 30 min, and then the amino acid **1** (180 mg) and the 3,5-dimetoxiabenzaldehyde **2b** (180 mg) were added portionwise (45 mg every 24 h), and the reaction mixture was heated at 115 °C for 5 days. After being cooled to room temperature, the solution was filtered on a Millipore membrane (PTFE, 0.22 μm), and the black solid was washed several times with fresh DMF, MeOH, and CH_2Cl_2 (sonicated, centrifuged, and filtered) until the supernatant solution remained colorless. The solid on the filter was washed with diethyl ether, affording functionalized SWNTs **5**

(27 mg). One functional group, each 129 atoms of carbon (21%), is calculated after analysis of TGA thermographs.

Sample Preparation. For the spectroscopic investigations, the SWNT samples were prepared in two different kinds of procedures. For SWNT/DMF, sample preparation was carried out by adding SWNT (0.5 mg) carefully to 10 mL of DMF followed by strong stirring overnight to presuspend SWNTs. The samples were then treated by a few cycles of temperature-controlled ultrasonic (112 W) for 30 min and vigorous stirring for 1 h. After that, unstably suspended material and large bundles were removed by slight centrifugation (2000*g*, 10 min). The resulting deep blackish stable supernatant was taken and again treated by temperature-controlled ultrasonic (112 W) for 30 min. The resulting suspensions were used for further investigations. For SWNT/SDBS samples, 0.5 mg of SWNT was added to 10 mL of SDBS/D_2O (0.1 M, 0.35 g of SDBS in 10 mL of D_2O) solution followed by strong stirring overnight to presuspend SWNTs. After that, we treated the suspension by five cycles of temperature-controlled ultrasonic (112 W) for 30 min and vigorous stirring for 1 h. Next, ultracentrifugation (21 000*g*, 30 min) was used to ensure the separation of well debundled SWNT. The resulting deep black supernatant was taken and was again treated by temperature-controlled ultrasonic (112 W) for 30 min. The resulting stable black suspensions were set to an equal optical density of 0.35 at 685 nm and were ready for using in further investigations. For spectroelectrochemical measurements, SWNTs (0.5 mg) and 0.1 mg of SDBS were stirred vigorously overnight in a solution (10 mL) of 0.1 M tetrabutylammonium hexafluorophosphate ($TBAPF_6$) that was dissolved in DMSO. To remove O_2, we degassed with Ar. Subsequently, the samples were sonicated (112 W) for not more than 30 min at 20 °C and kept for 60 min to separate larger aggregates. The resulting stable and deep black SWNT dispersion was added directly in our homemade spectroelectrochemical cell.

Chemicals. Solvents were purchased from Deutero and Fluka. All dry solvents were freshly distilled under argon over an appropriate drying agent before use. Chemicals were purchased from Sigma-Aldrich or Across Organics and were used as received without further purification. Aminoacid **1** was synthesized following the literature procedure. HiPco SWNTs were purchased from Carbon Nanotechnologies Inc. lot #R0496 and used without purification.

■ ASSOCIATED CONTENT

Supporting Information. Detailed characterization data for all compounds. This material is available free of charge via the Internet at http://pubs.acs.org.

■ AUTHOR INFORMATION

Corresponding Author
prato@units.it; guldi@chemie.uni-erlangen.de

■ ACKNOWLEDGMENT

This work was carried out with financial support from the Deutsche Forschungsgemeinschaft, Cluster of Excellence "Engineering of Advanced Materials", ICMM, ZMP "Zentralinstitut für Neue Materialien und Prozesstechnik", FCI, the Office of Basic Energy Sciences of the U.S., University of Trieste, INSTM, and MIUR (PRIN 2008, prot. 20085M27SS). Claudio Gamboz (Centro Servizi Polivalenti di Ateneo, Università Trieste) is gratefully acknowledged for assistance with TEM imaging. We acknowledge Jenny Malig (Department of Chemistry and Pharmacy & Interdisciplinary Center for Molecular Materials, Friedrich-Alexander-Universität Erlangen-Nürnberg) for the AFM measurements and for assistance. M.A.H. acknowledges support by the Junta de Comunidades de Castilla la Mancha (Spain) through the award of a postdoctoral fellowship.

■ REFERENCES

(1) (a) *Carbon Nanotubes: Advanced Topics in the Synthesis, Structure, Properties and Applications*; Jorio, A., Dresselhaus, G., Dresselhaus, M. S., Eds.; Springer: Berlin, 2008. (b) *Carbon Nanotubes: Synthesis, Structure, Properties and Applications*; Dresselhaus, M. S., Dresselhaus, G., Avouris, P., Eds.; Springer: Berlin, 2001. (c) Tanaka, K.; Yamabe, T.; Fukui, K. *The Science and Technology of Carbon Nanotubes*; Elsevier: Oxford, 1999. (d) Harris, P. J. F. *Carbon Nanotubes and Related Structures: New Materials for the Twenty-First Century*; Cambridge University Press: Cambridge, 2001. (e) *Carbon Nanotubes and Related Structures*; Guldi, D. M., Martin, N., Eds.; Wiley VCH: New York, 2010. (f) Charlier, J. C.; Issi, J. P. *J. Phys. Chem. Solids* **1996**, *57*, 957–965.

(2) (a) Guldi, D. M.; Rahman, G. M. A.; Sgobba, V.; Kotov, N. A.; Bonifazi, D.; Prato, M. *J. Am. Chem. Soc.* **2006**, *128*, 2315–2323. (b) Endo, M.; Iijima, S.; Dresselhaus, M. S. *Carbon Nanotubes*; Elsevier: Oxford, 1996.

(3) (a) Reich, S.; Thomsen, C.; Maultzsch, J. *Carbon Nanotubes: Basic Concepts and Physical Properties*; Wiley-VCH: Weinheim, 2004. (b) Rotkin, S. V.; Subramoney, S. *Applied Physics of Carbon Nanotubes: Fundamentals of Theory, Optics and Transport Devices*; Springer: Berlin, 2005. (c) Dresselhaus, M. S.; Eklund, P. C. *Adv. Phys.* **2000**, *49*, 705–814.

(4) (a) Lambin, P.; Meunier, V.; Henrard, L.; Lucas, A. A. *Carbon* **2000**, *38*, 1713–1721. (b) Marquis, R.; Greco, C.; Sadokierska, I.; Lebedkin, S.; Kappes, M. M.; Michel, T.; Alvarez, L.; Sauvajol, J.-L.; Meunier, S.; Mioskowski, C. *Nano Lett.* **2008**, *8*, 1830–1835. (c) Chen, Z.; Thiel, W.; Hirsch, A. *ChemPhysChem* **2003**, *4*, 93–97. (d) Niyogi, S.; Hamon, M. A.; Hu, H.; Zhao, B.; Bhowmik, P.; Sen, R. *Acc. Chem. Res.* **2002**, *35*, 1105–1113.

(5) (a) Bahr, J. L.; Mickelson, E. T.; Bronikowski, M. J.; Smalley, R. E.; Tour, J. M. *Chem. Commun.* **2001**, 193–194. (b) Ausman, K. D.; Piner, R.; Lourie, O.; Ruoff, R. S.; Korobov, M. *J. Phys. Chem. B* **2000**, *104*, 8911–8915. (c) Strano, M. S.; Moore, V. C.; Miller, M. K.; Allen, M. J.; Haroz, E. H.; Kittrell, C.; Hauge, R. H.; Smalley, R. E. *Science* **2003**, *301*, 1519–1522.

(6) (a) Fujigaya, T.; Nakashima, N. *Polym. J.* **2008**, *40*, 577–589. (b) Bergin, S. D.; Sun, Z.; Rickard, D.; Streich, P. V.; Hamilton, J. P.; Coleman, J. N. *ACS Nano* **2009**, *3*, 2340–2350. (c) Moonoosawmy, K. R.; Kruse, P. *J. Am. Chem. Soc.* **2008**, *130*, 13417–13424.

(7) (a) Tasis, D.; Tagmatarchis, N.; Bianco, A.; Prato, M. *Chem. Rev.* **2006**, *106*, 1105–1136. (b) Li, H.; Martin, R. B.; Harruff, B. A.; Carino, R. A.; Allard, L. F.; Sun, Y.-P. *Adv. Mater.* **2004**, *16*, 896–900. (c) Baskaran, D.; Ways, J. W.; Zhang, X. P.; Bratcher, M. S. *J. Am. Chem. Soc.* **2005**, *127*, 6916–6917. (d) Singh, P.; Campidelli, S.; Giordani, S.; Bonifazi, D.; Bianco, A.; Prato, M. *Chem. Soc. Rev.* **2009**, *38*, 2214–2230. (e) Brunetti, F. G.; Herrero, M. A.; Munoz, J. M.; Diaz-Ortiz, A.; Alfonsi, J.; Meneghetti, M.; Prato, M.; Vazquez, E. *J. Am. Chem. Soc.* **2008**, *130*, 8094–8100.

(8) (a) Murakami, H.; Nomura, T.; Nakashima, N. *Chem. Phys. Lett.* **2003**, *378*, 481–485. (b) Chen, J.; Collier, C. P. *J. Phys. Chem. B* **2005**, *109*, 7605–7609. (c) Li, H. P.; Zhou, B.; Lin, Y.; Gu, L.; Wang, W.; Fernando, K. A. S.; Kumar, S.; Allard, L. F.; Sun, Y. *J. Am. Chem. Soc.* **2004**, *126*, 1014–1015. (d) Hasobe, T.; Fukuzumi, S.; Kamat, P. V. *J. Am. Chem. Soc.* **2005**, *127*, 11884–11885. (e) Nakashima, N.; Tomonari, Y.; Murakami, H. *Chem. Lett.* **2002**, *31*, 638–639. (f) Chen, R. J.; Zhang, Y.; Wang, D.; Dai, H. *J. Am. Chem. Soc.* **2001**, *123*, 3838–3839. (g) Guldi, D. M.; Rahman, G. M. A.; Sgobba, V.; Ehli, C. *Chem. Soc. Rev.* **2006**, *35*, 471–487. (h) Britz, D. A.; Khlobystov, A. N. *Chem. Soc. Rev.* **2006**, *35*, 637–659. (i) Schuster, D. I.; Megiatto, J. D. *Nat. Chem.* **2009**, *1*, 182–183.

(9) Guldi, D. M.; Rahman, G. M. A.; Jux, N.; Tagmatarchis, N.; Prato, M. *Angew. Chem., Int. Ed.* **2004**, *43*, 5526–5530.

(10) Sgobba, V.; Rahman, G. M. A.; Guldi, D. M.; Jux, N.; Campidelli, S.; Prato, M. *Adv. Mater.* **2006**, *18*, 2264–2269.

(11) (a) Mateo-Alonso, A.; Ehli, C.; Chen, K. H.; Guldi, D. M.; Prato, M. *J. Phys. Chem. A* **2007**, *111*, 12669–12673. (b) Backes, C.; Schmidt, C. D.; Hauke, F.; Bottcher, C.; Hirsch, A. *J. Am. Chem. Soc.* **2009**, *131*, 2172–2184.

(12) (a) Guldi, D. M.; Marcaccio, M.; Paolucci, D.; Paolucci, F.; Tagmatarchis, N.; Tasis, D.; Vázquez, E.; Prato, M. *Angew. Chem., Int. Ed.* **2003**, *42*, 4206–4209. (b) Guldi, D. M.; Rahman, G. M. A.; Zerbetto, F.; Prato, M. *Acc. Chem. Res.* **2005**, *38*, 871–878. (c) Kordatos, K.; Da Ros, T.; Bosi, S.; Vazquez, E.; Bergamin, M.; Cusan, C.; Pellarini, F.; Tomberli, V.; Baiti, B.; Pantarotto, D.; Georgakilas, V.; Spalluto, G.; Prato, M. *J. Org. Chem.* **2001**, *66*, 4915–4920.

(13) Pang, L. S. K.; Saxby, J. D.; Chatfield, S. P. *J. Phys. Chem.* **1993**, *97*, 6941–6942.

(14) (a) Ehli, C.; Oelsner, C.; Guldi, D. M.; Mateo-Alonso, A.; Prato, M.; Schmidt, C.; Baches, C.; Hauke, F.; Hirsch, A. *Nat. Chem.* **2009**, *1*, 243–249. (b) Oelsner, C.; Schmidt, C.; Hauke, F.; Prato, M.; Hirsch, A.; Guldi, D. M. *J. Am. Chem. Soc.* **2011**, *133*, 4580–4586. (c) Iurlo, M.; Paolucci, D.; Marcaccio, M.; Paolucci, F. *Chem. Commun.* **2008**, 4867–4874.

(15) Quite different are the spectroscopic changes when scanning the oxidative range from 0 to 0.4 V and back to 0 V (vs Ag wire). Most importantly, in contrast to the reduction experiments, we note that an overall increase in the 1000−1600 nm absorption evolves synchronously, while shifting the potentials from 0 to 0.4 V (vs Ag wire). As in the reduction experiments, the van Hove singularities give rise to shifts, but they shift oppositely, to the red. Interestingly, this trend is much stronger under oxidative than under reductive conditions.

(16) (a) O'Connell, M. J.; Bachilo, S. M.; Huffman, C. B.; Noore, V. C.; Strano, M. S.; Haroz, E. H.; Rialon, K. R.; Boul, P. J.; Noon, W. H.; Kittrell, C.; Ma, J.; Hauge, R. H.; Weisman, R. B.; Smalley, R. E. *Science* **2002**, *297*, 593–596. (b) Bachilo, S. M.; Strano, M. S.; Kittrell, C.; Hauge, R. H.; Smalley, R. E.; Weisman, R. B. *Science* **2002**, *298*, 2361–2366. (c) Lefebvre, J.; Homma, Y.; Finnie, P. *Phys. Rev. Lett.* **2003**, *90*, 217401. (d) Lebedkin, S.; Hennrich, F.; Skipa, T.; Kappes, M. M. *J. Phys. Chem. B* **2003**, *107*, 1949–1956. (e) Lefebvre, J.; Homma, Y.; Finnie *Appl. Phys. A: Mater. Sci. Process.* **2004**, *78*, 1107–1110. The simulation and assignment of the spectral peaks was provided by HORIBA Jobin Yvon's Nanosizer software package.

(17) (a) Tanaka, Y.; Hirana, Y.; Niidome, Y.; Kato, K.; Saito, S.; Nakashima, N. *Angew. Chem., Int. Ed.* **2009**, *48*, 7655–7659. (b) Lin, Y.-Y.; Hung, W.-C.; Wai, C. M. *J. Phys. Chem. C* **2011**, *115*, 10561–10568.

(18) (a) Wang, F.; Dukovic, G.; Brus, L. E.; Heinz, T. F. *Phys. Rev. Lett.* **2004**, *92*, 177401. (b) Wang, F.; Dukovic, G.; Knoesel, E.; Brus, L. E.; Heinz, T. *QELS '05 In Quantum Electronics and Laser Science Conference*, 2005; Vol. *1*, pp 498−500.

(19) (a) Ehli, C.; Guldi, D. M.; Herranz, M. A.; Martín, N.; Campidelli, S.; Prato, M. *J. Mater. Chem.* **2008**, *18*, 1498–1503. (b) Herranz, M. A.; Martín, N.; Ramey, J.; Guldi, D. M. *J. Am. Chem. Soc.* **2008**, *130*, 66–73.

(20) (a) Ballesteros, B.; Campidelli, S; de la Torre, G.; Ehli, C.; Guldi, D.; Prato, Maurizio, M.; Torres, T. *Chem. Commun.* **2007**, 2950–2952. (b) Ballesteros, B.; de la Torre, G.; Ehli, C.; Aminur Rahman, G. M.; Agullo-Rueda, F.; Guldi, D. M.; Tomas, T. *J. Am. Chem. Soc.* **2007**, *129*, 5061–5068.

(21) Spectroscopic support for this assumption came from determining the absolute spectrum of the product and comparing it with that of the ground state. To this end, we conclude that the van Hove singularities shift indeed to the red.

(22) Faraggi, M.; Weinraub, D.; Broitman, F.; DeFelippis, M. R.; Klapper, M. H. *Radiat. Phys. Chem.* **1988**, *32*, 293.